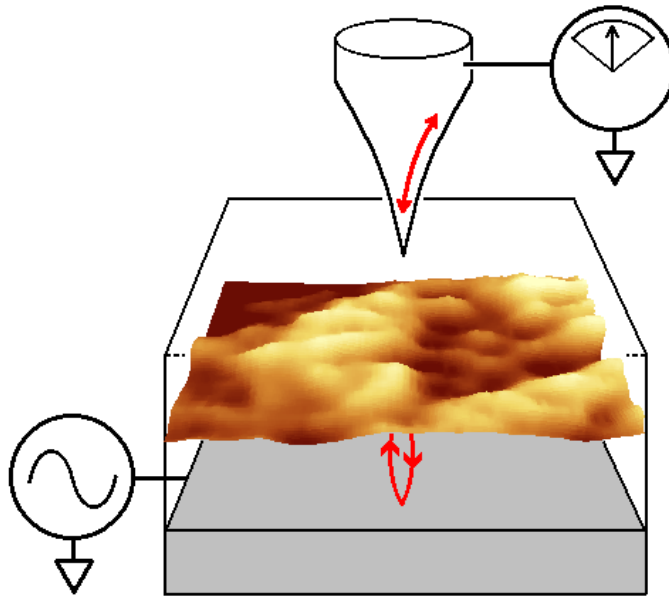


Direct Observation of Micron-Scale Ordered Structure in a Two-Dimensional Electron System

I. J. Maasilta[†], Subhasish Chakraborty, I. Kuljanishvili, and S. H. Tessmer
*Department of Physics and Astronomy, Michigan State University,
East Lansing, MI 48824*

M. R. Melloch
*Department of Electrical Engineering, Purdue University,
West Lafayette, Indiana 47907*



ABSTRACT

We have applied a novel scanned probe method to directly resolve the interior structure of a semiconductor two-dimensional electron system in a tunneling geometry. We find that the application of a perpendicular magnetic field can induce striking features. Near magnetic fields corresponding to six filled Landau levels, the structure forms distinct parallel lines that are not static as a function of the field, and extend as long as 5 μm . In some areas, overlapping sets of lines are observed. Present theories do not account for ordered density modulations on this length scale.

[†] *Current Address: Dept. of Physics, Univ. of Jyväskylä, FIN-40351 Jyväskylä, Finland.*
PACS numbers: 73.43.Jn, 73.43.Fj, 73.20.-r

Two-dimensional electron systems (2DES) formed in GaAs/AlGaAs heterostructures represent an ideal laboratory to study many-particle physics in lower dimensions [1]. Under various conditions, electron-electron interactions may result in ordered inhomogeneous states. The Wigner crystal represents a classic example, arising from direct Coulomb repulsion at sufficiently low density, temperature, and disorder [2]. In an applied perpendicular magnetic field, more general charge density wave (CDW) ground states are possible. The magnetic field B quantizes the kinetic energy into discrete, degenerate Landau levels; each spin-resolved level holds a density of eB/h electrons. At sufficiently high Landau level filling, Hartree-Fock based theories predict a CDW ground state of length scale on the order of the cyclotron radius, resulting from the competition between Coulomb repulsion and exchange attraction [3]. Recent transport measurements of high-mobility samples show that highly anisotropic dissipation occurs for more than four filled Landau levels, $\nu > 4$, with the uppermost level near half filling [4]. Unidirectional CDW stripes are believed to lie at the heart of these observations [5].

In contrast to transport measurements, scanned probe techniques sensitive to electric fields can provide direct images of GaAs/AlGaAs electronic structure [6]. In this Letter, we present an extension of Subsurface Charge Accumulation (SCA) imaging [7, 8], adapted to probe the 2DES interior in a novel tunneling geometry. The measurement works as follows: A tunneling barrier separates the 2D layer and a parallel 3D substrate. An *ac* excitation voltage applied between the substrate and a sharp metal tip locally induces charge to tunnel back and forth between the 3D and 2D layers. The measured signal is the resulting *ac* image charge on the tip electrode, which is proportional to the number of electric field lines terminating on it. No charge tunnels directly onto the tip. In this way, the experiment provides a local measurement of the ability of the 2D system to accommodate additional electrons. To the best of our knowledge, these data represent the first tunneling images of the interior of a GaAs/AlGaAs 2DES. At particular magnetic fields, striking micron-scale features are observed, corresponding to ordered electronic density modulations.

Our method can be considered as a locally resolved version of the pioneering work of Ashoori and coworkers [9], and Eisenstein and coworkers (in a 2D-2D tunneling geometry) [10]. These measurements and others (see for example [11, 12]) have demonstrated that the tunneling signal into a 2DES is sensitive to both gaps in the energy spectrum at integer Landau level fillings, and a Coulomb pseudogap that is pinned to the Fermi level of the 2D system. The pseudogap develops as a consequence of electron-electron interactions, and is

believed to depend strongly on the nature of localization of the electrons [13]. It is detected as an increase in the tunneling resistance, which is inversely proportional to the Fermi level tunneling density of states.

The sample used for these measurements was an $\text{Al}_{1.3}\text{Ga}_{7.7}\text{As}$ / GaAs (001) wafer grown by molecular beam epitaxy (MBE), shown schematically in Fig. 1(a). The 2DES is located at a distance of $d_1=60$ nm below the exposed surface, and a distance $d_2=40$ nm above a degenerately doped (10^{18} cm^{-3}) GaAs substrate (3D metal). The average electron density in the 2DES is $6 \times 10^{11} \text{ cm}^{-2}$, the low-temperature transport mobility is $\sim 10^5 \text{ cm}^2/\text{Vs}$, and the zero magnetic field 3D-2D tunneling rate is approximately 200 kHz. We position the tip to within a few nanometers of the sample surface using an innovative scanning head that provides a high degree of mechanical and thermal stability [14]. The image charge signal is detected using a circuit constructed from low-input-capacitance high-electron-mobility transistors (noise level 0.01 electrons/ $\sqrt{\text{Hz}}$). Most of the signal ($\sim 99.8\%$) corresponds to electric field emanating from areas macroscopically far from the

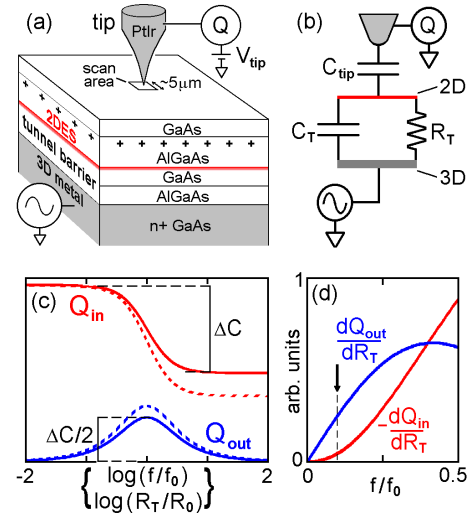


FIG. 1 (color). (a) Schematic of heterostructure sample and SCA measurement. The 2DES (indicated in red) forms in the potential well at the GaAs/AlGaAs interface from electrons provided by silicon dopants (+’s). An AlGaAs tunneling barrier separates the 2DES from a 3D substrate. (b) Equivalent circuit of the sample-tip system. (c) In-phase and 90° out-of-phase signals (Q_{in} and Q_{out}) versus frequency f and tunneling resistance R_T . The charging has identical functional dependence on f and R_T , with characteristic values of $f_0 = [2\pi R_T(C_T + C_{tip})]^{-1}$ and $R_0 = [2\pi f(C_T + C_{tip})]^{-1}$, respectively. The magnitude of the curves is set by the tip-sample capacitance difference ΔC between a fully charging and locally non-charging 2DES. The dashed curves qualitatively show the enhancements in Q_{in} and Q_{out} as the in-plane relaxation rates approach the tunneling rate. (d) A linear plot of the derivatives of Q_{in} and Q_{out} with respect to tunneling resistance. In the low-frequency limit of this experiment (arrow), the out-of-phase component is more sensitive to R_T variations.

location under the probe [15]. We subtract away this background signal using a bridge circuit. To acquire images, the tip is scanned laterally across the surface without the use of feedback. Unless otherwise noted, all measurements shown in this Letter were acquired with the system immersed in liquid helium-3 at a temperature of 270 mK, with a 20 kHz applied excitation voltage of 8 mV rms.

Fig. 1(b) shows a simple equivalent circuit for the measurement: The local contribution to the signal is modeled as a tip-2DES capacitance C_{tip} in series with the tunneling barrier, represented as a capacitor C_T and resistor R_T in parallel. To account for phase shifts we define two amplitudes Q_{in} and Q_{out} , representing respectively the in-phase and 90° out-of-phase (lagging) components of the image charge per unit excitation voltage. The typical units are attofarads ($1 \text{ aF} = 10^{-18} \text{ C/V}$). Fig. 1(c) shows the charging characteristics of the circuit. In zero magnetic field, the 20 kHz excitation frequency is about one-tenth of the tunneling rate across the barrier; i.e., $ff_0 \approx 0.1$. In this frequency range, the out-of-phase component is more sensitive to variations in the local tunneling resistance. This is shown in Fig. 1(d), which displays the derivatives of Q_{in} and Q_{out} with respect to R_T . In contrast, the in-phase component is mostly sensitive to capacitance variations in the low-frequency limit (not shown), including the compressibility contribution to the capacitance [15, 16]. More rigorous models for the system consider the distributed nature of the tip-sample capacitance and the effect of charge motion within the 2D plane [17]. Such models show an enhancement in the charging characteristics as the 2DES becomes an increasingly poor conductor, i.e., as the system approaches integer filling, as indicated qualitatively by the dashed curves in Fig. 1(c).

Fig. 2(a) shows a basic measurement performed at $B=0$ with the tip held at a fixed location. As a function of the dc tip voltage V_{tip} , Q_{in} forms a step-like curve with a clear drop near 0 V. This indicates that the tip acts as a gate electrode that can locally deplete the 2DES. In depletion, charge cannot tunnel into the 2D layer under the apex; hence the local contribution to the signal shifts from the tip-2DES capacitance to the lower tip-substrate value. The arrow marks the contact potential, $V_{null} = 0.60 \text{ V}$, as determined by *in situ* Kelvin Probe measurements [7]. All SCA data shown below were acquired at $V_{tip} = V_{null}$, so that the tip itself does not produce a dc perturbation of the 2DES [18]. From the magnitude of the capacitance step, we can estimate the measurement's spatial resolution. Applying a parallel plate model for C_{tip} and C_T , ΔC can be written as $\Delta C = A\kappa\epsilon_0[1/d_1 - 1/(d_1+d_2)] = 15 \text{ aF}$, where $\kappa = 12.5$ is the AlGaAs

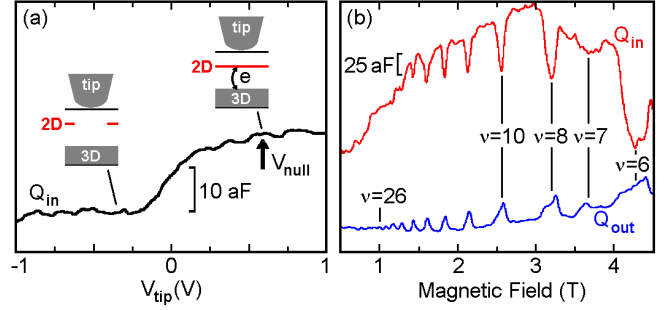


FIG. 2 (color). Fixed tip measurements. (a) At zero magnetic field the signal displays a step-like curve as a function of dc bias voltage. This indicates the local depletion of the 2DES for negative tip potential. (b) As a function of perpendicular magnetic field, Q_{in} and Q_{out} display clear features at integer Landau level fillings, as indicated.

dielectric constant. Solving for the area yields $A = 2.0 \times 10^{-14} \text{ m}^2$, or a radius of 80 nm. This value is comparable to both the tip-2DES distance, and the nominal 50 nm radius of curvature of our chemically etched PtIr tips, parameters that are expected to set the length scale for the measurement.

Fig. 2(b) shows fixed-tip charging as a function of magnetic field, acquired using the same tip as for the subsequent images. Both the in-phase and out-of-phase curves (acquired simultaneously) exhibit sensitivity to Landau level structure with $1/B$ periodicity. The dips in the in-phase curves reflect a reduction in capacitance caused by the diminished compressibility of the 2D system at integer filling. With respect to the out-of-phase component, the peaks at integer filling likely reflect an increase of the pseudo gap, resulting in an increased tunneling resistance [12]. As shown in Fig. 1(d), this causes Q_{out} to increase in the low-frequency limit. In addition, reduced in-plane conductivity may also contribute.

Fig. 3(a) presents two sets of charging images, acquired at two different values of B far from integer filling, i.e., fields where no Q_{out} peaks were observed in fix-tip measurements. The in-phase data show a charging pattern that remains largely unchanged, irrespective of the value of B . This phenomenon was observed in all the data sets. In some cases we measured constant in-phase charging patterns for more than 100 hours (the hold-time of our cryostat), a testament to the stability of the microscope and sample.

We attribute the structure seen in Q_{in} to surface topography, which modulates the geometric capacitance and couples preferentially to Q_{in} in the low-frequency limit. This conclusion is supported by comparison to a surface topography measurement (at a different location) acquired by operating the microscope in a standard scanning tunneling microscopy mode [14]. As shown in Fig. 3(b), the surface consists of elongated mounds

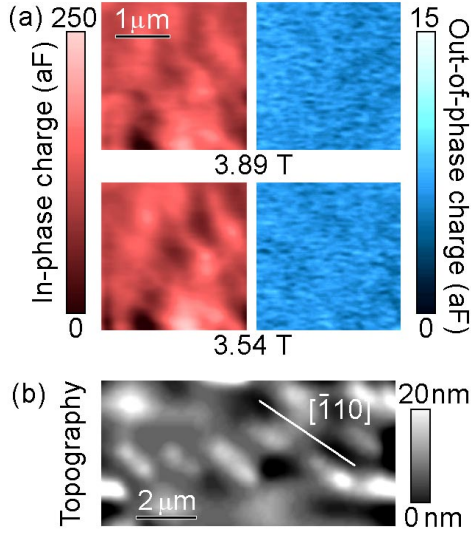


FIG. 3 (color). (a) Q_{in} (left) and Q_{out} (right) images acquired at two magnetic fields where no features were seen in the fixed-tip data. A time difference of six hours elapsed between the acquisition of the two data sets. (b) Topographical surface image showing the orientation of the growth features. The image was acquired at room temperature without altering the orientation of the crystal. The elongated mounds are about 5 nm tall, and typically point along the $[\bar{1}10]$ direction, as indicated approximately by the white line.

qualitatively similar to the in-phase structure. These surface features typically point along the $[\bar{1}10]$ direction, as indicated, reflecting an MBE growth instability [19]. In contrast to the in-phase patterns, the out-of-phase images show only a slight topographical contribution, as expected in the low-frequency limit, which we subtract away. Far from integer filling, no significant features remain in Q_{out} discernible above the background noise, as shown in Fig. 3(a).

As the magnetic field approaches integer filling $\nu=6$, we observe completely different behavior for the Q_{out} images. Clear and reproducible features appear that are not correlated with the Q_{in} signal, as seen in Fig. 4. Some of the structures appear as round micron scale droplets, such as the bright feature in the upper left corner of the 4.32 T image of Fig. 4(b). These are qualitatively similar to droplet structures observed in reference [7], and to potential contours mapped out in reference [8]. In addition, we focus on features in the images that form micron-scale parallel lines. To clearly point out examples of linear features, the 4.14 T and 4.08 T images are reproduced in Fig. 4(c). The arrows mark three dark (reduced-charging) features that form parallel lines, two of which extend for more than 5 μm . Fig. 4(d) shows an enlargement of the 4.08 T data corresponding to the dashed box of Fig. 4(c). In this image, a striking triangular pattern can be identified. We

interpret the pattern as emerging from three sets of micron-scale lines.

Similar to the out-of-phase peaks of Fig. 2(b), the imaged Q_{out} structure may result from local variations of the pseudo gap and/or in-plane conductivity. In either case, we can identify the structure as originating from modulations in the 2DES density which bring the system slightly closer and further from integer filling as a function of lateral position. We believe the droplet shaped features reflect density modulations induced by the static disorder potential, consistent with the interpretation of references [7] and [8]. This view is also consistent with observations we have made of droplet

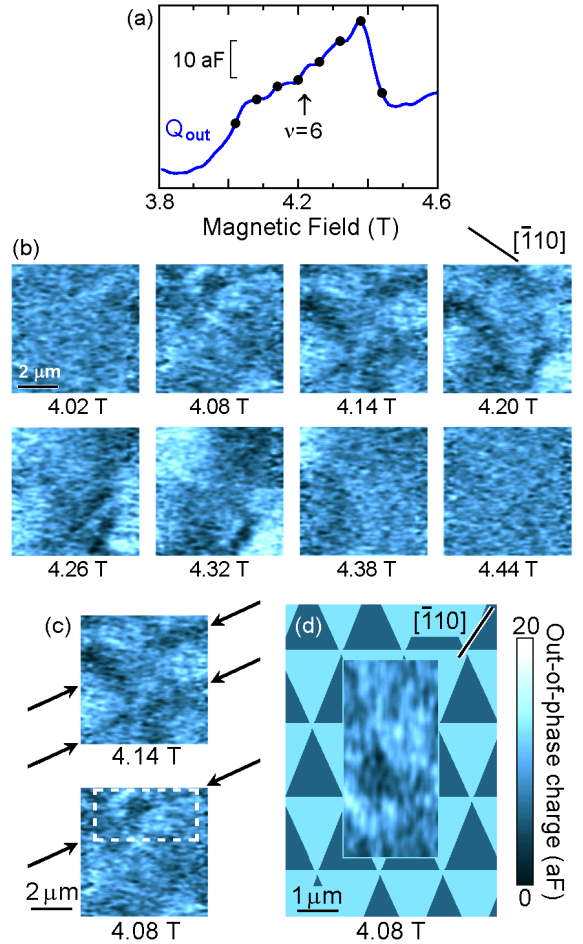


FIG. 4 (color). Out-of-phase data near $\nu=6$. (a) A fixed-tip Q_{out} curve displaying the $\nu=6$ peak, acquired near the upper right corner of the imaged area. (b) A series of 6 $\mu\text{m} \times 6 \mu\text{m}$ images for eight fields, indicated as dots in (a). The topographical contribution to each image has been subtracted. The approximate crystallographic direction $[\bar{1}10]$ is indicated. (c) Images at two selected magnetic fields. The arrows point to linear features of lower out-of-phase charging. (d) Enlargement of the area shown in the dash box at 4.08 T in (c). The image has been rotated 90° counterclockwise; a schematic triangular pattern is shown around the border as a guide to the eye. All images are displayed with the same color scale, shown at the lower right.

features that reappeared and evolved in a similar manner at both $\nu=6$ and $\nu=7$. With regard to the linear features, we have observed similar patterns near $\nu=6$ and $\nu=4$, in different areas of the sample. The fact that the structures shift position and evolve considerably with magnetic field argues against static potential variations (or tunneling barrier nonuniformity) as the origin. Moreover, Kelvin Probe images of the same areas show no indications of the linear features. Hence, we conclude that these structures do not simply mirror static charges in the donor layer or sample surface.

In conclusion, we have obtained the first direct images of ordered structure within the interior of a GaAs/AlGaAs 2DES using a novel scanned probe method. It is tempting to equate the observations with states similar to the theoretical Hartree-Fock high-Landau-level CDW's [3]. However, the length scales represent a major discrepancy: we observe structures on the scale of $\sim 2 \mu\text{m}$, whereas current theories predict a characteristic length of $\sim 100 \text{ nm}$, set by the cyclotron radius. We speculate that interplay with micron scale disorder may cause a larger length scale to be selected. Conversely, the observed length scale may arise spontaneously from physics unanticipated by theory.

We thank R. C. Ashoori, J. Bass, H.-B. Chan, V. J. Goldman and S. Urazhdin for discussions and assistance. We gratefully acknowledge enlightening conversations with M. I. Dykman, A. H. MacDonald, and J. Sinova with regard to the interpretation of these data. This work was supported by the National Science Foundation (DMR-0075230). SHT acknowledges support of the Alfred P. Sloan Foundation.

1. H. L. Stormer, D. C. Tsui, A. C. Gossard, *Rev. Mod. Phys.* **71**, S298 (1999).
2. S. Das Sarma and A. Pinczuk, Eds., *Perspectives in Quantum Hall Effects* (Wiley, New York, 1997).
3. A. A. Koulakov, M. M. Fogler, and B. I. Shklovskii, *Phys. Rev. Lett.* **76**, 499 (1996); R. Moessner and J.T. Chalker, *Phys. Rev. B* **54**, 5006 (1996).
4. M. P. Lilly *et al.*, *Phys. Rev. Lett.* **82**, 394 (1999); W. Pan, *et al.*, *Phys. Rev. Lett.* **83**, 820 (1999); K. B. Cooper *et al.*, *cond-mat/0203174*.
5. A. H. MacDonald and M. P. A. Fisher, *Phys. Rev. B* **61**, 5724 (2000); E. Fradkin *et al.*, *Phys. Rev. Lett.* **84**, 1982 (2000); H. Fertig, *Phys. Rev. Lett.* **82**, 3693 (1999); E. H. Rezayi, F. D. M. Haldane, and K. Yang, *Phys. Rev. Lett.* **83**, 1219 (1999); D. V. Fil, *Low Temp. Phys.* **26**, 581 (2000).
6. K. L. McCormick *et al.*, *Phys. Rev. B* **59**, 4654 (1999); A. Yacoby *et al.*, *Solid State Commun.* **111**, 1 (1999); N. B. Zhitenev *et al.*, *Nature* **404**, 473 (2000); M. A. Topinka *et al.*, *Nature* **410**, 183 (2001).
7. S. H. Tessmer *et al.*, *Nature* **392**, 51 (1998).
8. G. Finkelstein *et al.*, *Science* **289**, 90 (2000).
9. R.C. Ashoori *et al.*, *Phys. Rev. Lett.* **64**, 681 (1990).
10. J. P. Eisenstein, L. N. Pfeiffer, and K. W. West, *Phys. Rev. Lett.* **69**, 3804 (1992).
11. K. M. Brown *et al.*, *Phys. Rev. B* **50**, 15 465 (1994); H. B. Chan *et al.*, *Phys. Rev. Lett.* **83**, 3258 (1999).
12. E. V. Deviatov *et al.*, *Phys. Rev. B* **61**, 2939 (2000).
13. A. H. MacDonald, *Solid State Commun.* **102**, 143 (1997), Section V, and references therein.
14. S. Urazhdin *et al.*, *Rev. Sci. Instrum.* **71**, 4170 (2000).
15. S. H. Tessmer *et al.*, *cond-mat/0203339*.
16. T. P. Smith *et al.*, *Phys. Rev. B* **32**, 2696 (1985).
17. I. J. Maasilta *et al.*, unpublished.
18. M. J. Yoo *et al.*, *Science* **276**, 579 (1997).
19. C. Orme *et al.*, *Appl. Phys. Lett.* **64**, 860 (1994); R. L. Willett *et al.*, *Phys. Rev. Lett.* **87**, 126803 (2001).